The Astrophysical Journal, 775:83 (13pp), 2013 October 1 doi:10.1088/0004-637X/775/2/83

MEAN AGE GRADIENT AND ASYMMETRY IN THE STAR FORMATION HISTORY OF THE SMALL MAGELLANIC CLOUD*

M. Cignoni[1,2], A. A. Cole[3], M. Tosi[2], J. S. Gallagher[4], E. Sabbi[5], J. Anderson[5], E. K. Grebel[6], and A. Nota[5,7]
[1] Astronomy Department, University of Bologna, I-Bologna 40127, Italy
[2] INAF-Bologna Observatory, I-Bologna 40127, Italy
[3] School of Mathematics & Physics, University of Tasmania, Private Bag 37, Hobart, Tasmania 7001, Australia; michele.cignoni@unibo.it
[4] University of Wisconsin, Madison, WI, USA
[5] STScI, Baltimore, MD 21218, USA
[6] Astronomisches Rechen-Institut, Zentrum für Astronomie der Universität Heidelberg, Mönchhofstr. 12–14, D-69120 Heidelberg, Germany
[7] European Space Agency, Research and Scientific Support Department, Baltimore, MD, USA
Received 2013 May 20; accepted 2013 July 31; published 2013 September 6

ABSTRACT

We derive the star formation history (SFH) in four regions of the Small Magellanic Cloud (SMC) using the deepest *VI* color–magnitude diagrams (CMDs) ever obtained for this galaxy. The images were obtained with the Advanced Camera for Surveys on board the *Hubble Space Telescope* (*HST*) and are located at projected distances of 0.°5–2° from the SMC center, probing the main body and the wing of the galaxy. We derived the SFHs of the four fields using two independent procedures to fit synthetic CMDs to the data. We compare the SFHs derived here with our earlier results for the SMC bar to create a deep pencil-beam survey of the global history of the central SMC. We find in all the six fields observed with *HST* a slow star formation (SF) pace from 13 to 5–7 Gyr ago, followed by a ≈2–3 times higher activity. This is remarkable because dynamical models do not predict a strong influence of either the Large Magellanic Cloud (LMC) or the Milky Way at that time. The level of the intermediate-age SF rate enhancement systematically increases toward the center, resulting in a gradient in the mean age of the population, with the bar fields being systematically younger than the outer ones. SF over the most recent 500 Myr is strongly concentrated in the bar, the only exception being the area of the SMC wing. The strong current activity of the latter is likely driven by interaction with the LMC. At a given age, there is no significant difference in metallicity between the inner and outer fields, implying that metals are well mixed throughout the SMC. The age–metallicity relations we infer from our best-fitting models are monotonically increasing with time, with no evidence of dips. This may argue against the major merger scenario proposed by Tsujimoto and Bekki in 2009, although a minor merger cannot be ruled out.

Key words: galaxies: dwarf – galaxies: evolution – galaxies: formation – galaxies: individual (Small Magellanic Cloud) – galaxies: star formation – galaxies: stellar content – galaxies: structure – Hertzsprung–Russell and C–M diagrams – Magellanic Clouds – stars: statistics

Online-only material: color figures

1. INTRODUCTION

This paper is one of a series devoted to the derivation of the star formation history (SFH) of the Small Magellanic Cloud (SMC) from the comparison of deep, high-resolution color–magnitude diagrams (CMDs) of its resolved stars with synthetic CMDs based on stellar evolution models.

It is part of a long-term project aimed at studying the evolution of the SMC in space and time, using the *Hubble Space Telescope* (*HST*), the Very Large Telescope (VLT), and the Guaranteed Time at the VLT Survey Telescope (VST) to observe a large sample of field stars and clusters across the SMC (see, e.g., Nota et al. 2006; Ripepi et al. 2006; Carlson et al. 2007; Sabbi et al. 2007, 2009; Glatt et al. 2008a, 2008b, 2011; Tosi et al. 2008; Cignoni et al. 2012). This extensive data set will allow us to constrain the global SFH as well as the existence of chemical and age gradients (if any) over the whole lifetime and spatial extent of the SMC.

The SMC is an excellent benchmark to study the evolution of late-type dwarf galaxies. It is the closest dwarf irregular (dIrr), has a current metallicity $Z \simeq 0.004$ (as derived from H II regions and young stars) similar to that of the majority of dIrr galaxies, and has a mass, estimated between 1 and $5 \times 10^9\ M_\odot$, at the upper limit of the range of this morphological class (Tolstoy et al. 2009, and references therein).

Thanks to the sensitivity and the large field of view of the VST, we will have CMDs a few magnitudes fainter than the oldest main-sequence turnoff (MSTO) for the entire galaxy and the Bridge connecting the SMC to the Large Magellanic Cloud (LMC). Meanwhile, we have already acquired deeper, higher-resolution photometry of four SMC young clusters (Nota et al. 2006), seven intermediate-age and old clusters (Glatt et al. 2008a, 2008b), and six fields (Sabbi et al. 2009) with the Advanced Camera for Surveys (ACS) on board *HST*.

We have chosen the six *HST* fields to sample regions characterized by different star formation (SF) activity and stellar and gas densities. They are located in the SMC bar, in the outskirts, and in the wing, i.e., the large cloud of faint stars protruding toward the LMC, which is considered to be part of a tidal tail

* Based on observations with the NASA/ESA *Hubble Space Telescope*, obtained at the Space Telescope Science Institute, which is operated by AURA, Inc., under NASA contract NAS 5-26555. These observations are associated with program GO-10396.

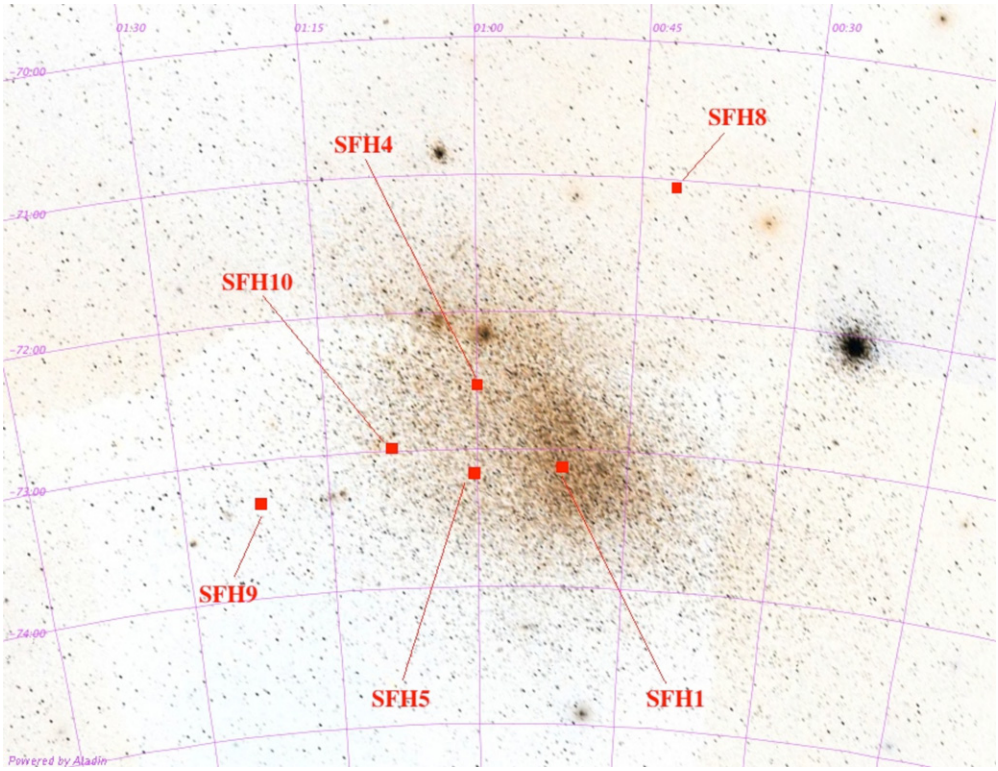

Figure 1. Spatial distribution of our six SMC fields observed with *HST*/ACS, superimposed on the Digital Sky Survey image of the SMC. North is up, and east is left. (A color version of this figure is available in the online journal.)

torn off the main body of the SMC by the interactions between the two Clouds (Westerlund 1964).

We derive the SFHs of the observed fields using the synthetic CMD technique (see, e.g., Tolstoy et al. 2009; Cignoni & Tosi 2010, and references therein). To estimate the intrinsic theoretical uncertainties, the SFH is derived using two completely independent procedures for the application of the synthetic CMD method: the Bologna code (see, e.g., Cignoni & Tosi 2010) and Andrew Cole's annealing procedure (Cole et al. 2007). We have summarized the two methods, their commonalities and differences, in the paper by Cignoni et al. (2012), where we applied them to the two most central *HST* fields of our sample of six. Those two fields are located in the SMC bar. Here we present the results for the remaining four *HST* fields: one (SFH10) between the bar and the wing, one (SFH9) in the wing, one (SFH5) in the "central system" (Westerlund 1997) but away from the bar, and one (SFH8) in the galaxy outskirts, at the same distance from the center as our wing field SFH9 but in the direction opposite to the LMC (see Figure 1).

SFHs of other SMC fields have been derived and presented by other groups, based on *HST* images of small individual regions or on ground-based photometry (see Figure 1 in Cignoni et al. 2012). Gardiner & Hatzidimitriou (1992) analyzed UKST plate data totaling 130 deg^2 around the SMC; this remains the largest areal coverage CMD analysis published to date, but does not reach below the horizontal branch (HB)/red clump (RC). By comparison, CCD studies have covered much smaller areas. Harris & Zaritsky (2004) derived the SFH of the SMC over $4^\circ \times 4.^\circ5$ to a depth of $V \lesssim 21$ using the Magellanic Cloud Photometric Survey *UBVI* catalog by Zaritsky et al. (2002). Recently, Nidever et al. (2011) published the first results from a $\approx$15 deg^2 survey covering selected fields at angular distances of 2°–11° from the SMC center defined by Mateo (1998), deep enough to reach the old MSTO in the uncrowded outer regions. Noël et al. (2007, 2009) presented a deep ground-based study of 12 fields of the SMC, avoiding the densest regions, because of their high crowding conditions.

HST studies have usually concentrated on regions of recent SF and/or high crowding. Dolphin et al. (2001) analyzed the stellar content at the outskirts of the SMC, in a region close to the globular cluster NGC 121, using both *HST* Wide Field Planetary Camera 2 (WFPC2) and ground-based data. McCumber et al. (2005) studied the stellar content of a small portion of the SMC wing also with the WFPC2. A summary of WFPC2 studies and reanalysis of the CMD data have been undertaken by Weisz et al. (2013). With ACS, Chiosi & Vallenari (2007) have derived the SFH in the vicinity of a few SMC clusters. Here, we perform a quantitative analysis of the fields located at a range of radial distances from the SMC center, described in Sabbi et al. (2009).

The layout of this paper is as follows: the *HST* data and resulting CMDs are briefly described in Section 2, while the SFH derivation with the two different procedures is presented in Section 3. Similarities and differences between the resulting SFHs are also discussed there. In Section 4 we compare our results with published literature on other SMC regions. Our conclusions close the paper.

2. *HST* PHOTOMETRY AND CMDs

Our six SMC fields were imaged in the F555W and F814W filters with the ACS Wide Field Channel (WFC) from 2005 November to 2006 January (GO-10396; P.I. Gallagher). The data reduction was performed with the program img2xym_WFC.09x10 (Anderson & King 2006), and the resulting magnitudes were calibrated in the Vegamag photometric

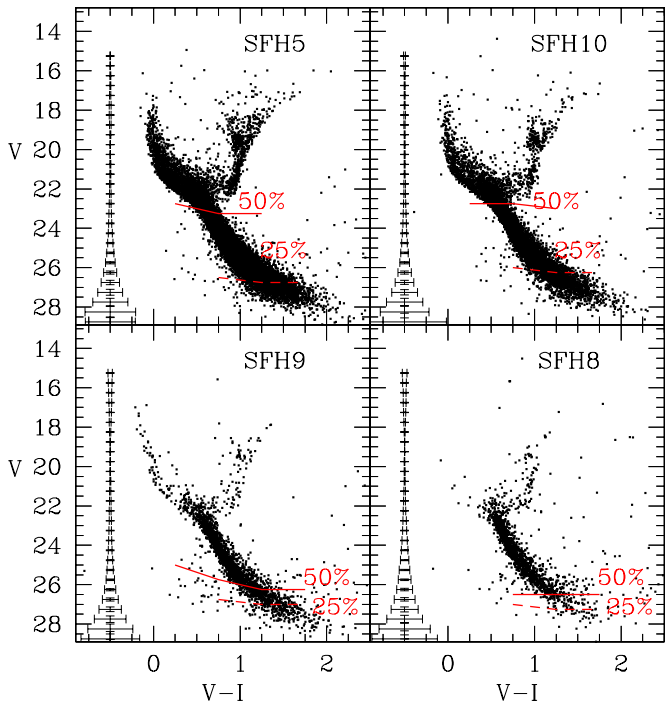

Figure 2. CMDs of the SFH5, SFH8, SFH9, and SFH10 fields observed with the ACS/WFC. The solid and dashed red lines indicate the 50% and 25% levels of completeness, respectively. Formal errors on the estimated photometry are shown on the left side of each CMD (see text for details).

(A color version of this figure is available in the online journal.)

system using Sirianni et al. (2005) prescriptions. For the sake of conciseness, from now on we will refer to the $m_{\rm F555W}$ and $m_{\rm F814W}$ magnitudes calibrated in the Vegamag system as V and I, respectively.

Extensive artificial star experiments were performed following the approach described in Anderson et al. (2008) to test the level of completeness and the photometric errors of the data. The artificial stars were searched for with exactly the same procedure adopted for the real stars. We considered an artificial star recovered if its input and output positions agreed to within 0.5 pixels and the fluxes agreed to within 0.75 mag. As done for the photometric analysis, we also required that each star is found in at least three exposures with a positional error <0.1 pixels filter^{-1}. Details on both the photometry and the artificial star tests can be found in Sabbi et al. (2009).

The final CMDs are shown in Figure 2, where the photometric errors are also plotted.[8] These CMDs show the superb tightness typical of *HST* photometry and reach almost 4 mag fainter than the oldest MSTO, thus allowing us to study the evolution of the regions over the whole Hubble time.

All four CMDs display well-populated sequences of all the evolutionary phases of old and intermediate-age stars: main sequence (MS), sub-giant branch (SGB), red giant branch (RGB), and RC. In addition to these components, all the CMDs except that of SFH8 present a bright blue plume typical of young, high- and intermediate-mass stars. None of the CMDs, with the possible exception of SFH9, show any significant population of pre-main-sequence (PMS) stars. This suggests a SF activity in the past 50 Myr much lower than that of the currently most active regions of the SMC, such as NGC 346 and NGC 602, where we measured many PMSs with the same observing setup (see, e.g., Nota et al. 2006; Carlson et al. 2007; Cignoni et al. 2009, 2010, 2011). None of the CMDs show evidence of an HB, suggesting that in all the fields the SF activity was quite low at epochs earlier than around 10 Gyr ago.

The CMDs differ from each other for some key features. First of all, the number of stars present in the CMD strongly depends on the apparent galactocentric distance of the region. The final photometric catalogs contain about 29,200 objects in SFH1, 17,300 in SFH4, 19,770 objects in SFH5, 1560 in SFH8, 2660 in SFH9, and 9180 in SFH10 (Sabbi et al. 2009). In practice, the most populated region is the most central one (SFH1). SFH4 and SFH5, with a similar projected distance from the SMC center, contain a similar number of stars, and the more external fields host much fewer objects.

The bar field SFH1 is the closest ($\sim$3′) to the SMC optical center defined by Gonidakis et al. (2009)[9] and contains $\sim$8.5 stars pc^{-2}. SFH4 is also in the bar, at $\sim$53′ from the SMC optical center, and has a stellar density of $\sim$5 stars pc^{-2}. SFH5 is located at $\sim$41′ from the center, but at right angles to the bar major axis; its density of $\sim$5.7 stars pc^{-2} is second only to the density in SFH1, emphasizing that while the bar is prominent in the younger populations, the older stars are more symmetrically distributed (see, e.g., Gardiner & Hatzidimitriou 1992 and Figures 2 and 3 in Zaritsky et al. 2000). SFH8 is $\sim$2°10′ north from the SMC optical center and has the lowest stellar density of all our *HST* fields, $\sim$0.5 stars pc^{-2}, almost a factor of 20 lower than in SFH1. SFH9 is located in Shapley's wing and is the region most distant in projection from the optical center of the SMC (2°14′) in our sample. Its stellar density is as low as $\simeq$0.8 stars pc^{-2}. Midway between the bar and wing, SFH10 lies 1°17′ from the center. Its stellar density is $\simeq$2.7 stars pc^{-2}, 3.5 times denser than SFH9 and 3.1 times less dense than SFH1, in good agreement with the slope of the surface brightness fit by Bothun & Thompson (1988).

In terms of populations, there is an obvious age difference between SFH8 and the others: it shows no blue plume of MS stars brighter than $V \approx 21$, even though it is well within the boundary of the area described by Nidever et al. (2011) as the "inner component" and by Westerlund (1997) as the "central system" (radius 3°–3.°5). In contrast, SFH9, although at an apparent slightly larger distance from the center, has a very narrow and well-defined blue plume, bluer at its bright end than any of the others. This is the locus of very young stars and implies that the most external parts of the wing are still forming stars, thus emphasizing the asymmetry of the activity in the SMC. The narrowness of the upper MS in SFH9 compared to the broad blue plumes in the more central fields emphasizes the likelihood that the wing represents a single SF event and not a spatial redistribution of the populations in the central regions.

3. SFH AND AGE–METALLICITY RELATION OF THE FOUR FIELDS

The SFHs of SFH5, SFH8, SFH9, and SFH10 have been derived with the synthetic CMD method following two independent procedures: Cole's (e.g., Cole et al. 2007) and Bologna's, the latter being a combination of the procedure developed by Cignoni (e.g., Cignoni 2006; Cignoni et al. 2006) with those

[8] To be conservative, the plotted error bars correspond at each magnitude level to the larger value of the error resulting from the photometric package and from the artificial star tests (which tend to be slightly larger than those based on point-spread function photometry alone).

[9] This center is found using K and M stars and hence provides a good estimate of the stellar mass distribution.

Table 1
Summary of SFH Solution Parameters[a]

Field	Method	$(m-M)_0$ (mag)	$E(B-V)$ (mag)	IMF	CMD binning (color × mag)	Metallicities ($Z \times 10^3$)
SFH5	Bologna	18.85	0.08[b]	Kroupa (2001)	variable	0.4,1, 2, 4
Central	Cole	18.95	0.07[b]	Chabrier (2003)	0.04 × 0.08	0.15, 0.4, 0.6, 1.0, 1.5, 2.4, 4.0
SFH10	Bologna	18.83	0.095[b]	Kroupa (2001)	variable	0.4, 1, 2, 4
Intermediate	Cole	18.89	0.06[b]	Chabrier (2003)	0.04 × 0.08	0.15, 0.4, 0.6, 1.0, 1.5, 2.4, 4.0
SFH9	Bologna	18.81	0.10	Kroupa (2001)	variable	0.4, 1, 2, 4
Wing	Cole	18.90	0.10	Chabrier (2003)	0.04 × 0.08	0.15, 0.4, 0.6, 1.0, 1.5, 2.4, 4.0
SFH8	Bologna	18.85	0.087	Kroupa (2001)	variable	0.4, 1, 2, 4
Outer	Cole	18.96	0.06	Chabrier (2003)	0.04 × 0.08	0.15, 0.4, 0.6, 1.0, 1.5, 2.4, 4.0

Notes.
[a] All models based on the Padova isochrone set; see text for details.
[b] Differential reddening assumed for stars younger than 500 Myr; see text for details.

defined and improved over the years at the Bologna Observatory (see Tosi et al. 1991; Greggio et al. 1998; Angeretti et al. 2005). Commonalities and differences of Cole's and Bologna's methods were summarized by Cignoni et al. (2012).

For these four fields we followed exactly the same procedures and assumptions as described in the latter paper for SFH1 and SFH4. In all cases, the synthetic CMDs have been built to reproduce the number of stars measured in the observational diagrams, using the results of the artificial star tests, described in the previous section, to assign photometric errors and incompleteness to the synthetic stars. The synthetic stars are simulated from the stellar evolution models computed by the Padova group (Bertelli et al. 2008, 2009) and converted directly to the *HST* Vegamag photometric system, to minimize the uncertainties related to calibration issues.

Initial mass function (IMF), binary fraction, reddening, differential reddening, and distance modulus in principle are allowed to vary freely, but in practice always turn out to be viable only within restricted ranges of value. No age–metallicity relation (AMR) is assumed a priori.

The best solution is searched in a statistical manner (χ^2 minimization over appropriate CMD grids with a downhill simplex algorithm in the Bologna case, and a simulated annealing approach for maximum likelihood based on Cash (1979) statistics in Cole's). The quantitative solutions are not truly unique although the optimization methods are both highly tuned to produce nearly formally unique results. By showing the results from both methods, we allow for a robust derivation of the range of parameter values that is more realistic than the error bars resulting from any single method.

Distances and reddenings are initially constrained to the values given in Sabbi et al. (2009), but are allowed to vary if the resulting synthetic CMDs do not optimally match the data. All the parameters of the SFH solutions for each field are summarized in Table 1.

The best-fit distances always correspond to distance moduli shorter than recently determined from eclipsing binaries ($(m-M)_0 = 19.11$; North et al. 2010), but still compatible with the average distance of RR Lyrae ($(m-M)_0 = 18.90$; Kapakos et al. 2011) and of star clusters (around 18.87 for Glatt et al. 2008b and between 18.71 and 18.82 for Crowl et al. 2001). These differences may be, at least partially, due to the line-of-sight depth variations found by Subramanian & Subramaniam (2009; up to 4.9 kpc) and Glatt et al. (2008b; between 10 and 17 kpc). Indeed, the old SMC population (as traced by RR Lyrae stars) has a mean depth of 4.2 ± 0.4 kpc (with maximum values up to 5.6 kpc). The young populations (as traced by Cepheids) show not only a radically different distribution but also higher depths: in total, a mean depth of 7.5 ± 0.3 kpc. In particular, several of the regions in which our *HST* fields are located belong to areas with very large line-of-sight depth values (see Figure 6 in Haschke et al. 2012). In addition, the orientation of the spatial distribution of the young SMC population is such that the northeastern part (where several of our *HST* fields are located) is closer to us than the rest (see Haschke et al. 2012).

Note that in each field the SFH solutions from the two different methods find systematically different distances, although the differences (≈0.1 mag = ≈3 kpc) are within both the likely errors and the physical depth of the cloud.

The best-fitting reddenings are in good agreement with the foreground value found by Schlegel et al. (1998). To better reproduce the color width of the upper MS, the solutions for SFH5 and SFH10 required a small amount of differential reddening: the Bologna solutions added an additional $E(B-V) = 0.02$ for stars younger than 500 Myr, while Cole added 0.02 to SFH5 and 0.03 to SFH10 for stars younger than 250 Myr. Indeed, reddening has been demonstrated to be highly variable and differential in the SMC (see, e.g., Zaritsky et al. 2002; Haschke et al. 2011).

In the next sections, Cole's and Bologna's best-fit solutions are presented as SFH#-C and SFH#-B, respectively (e.g., SFH5-C indicates Cole's SFH for SFH5), and compared with each other. Since SFH5 is the only field where Bologna and Cole solutions differ more than formal errors, for this region we will discuss the CMD residuals in some detail. For the other fields, where the resulting SFHs are well consistent within the uncertainties, we will show only the synthetic CMD corresponding to Bologna's solutions.

3.1. SFH5

SFH5 is the densest region of the four examined here and the second densest of all our six *HST* fields. In its CMD we find the signatures of both very old stars (the fainter SGB stars are at least 12 Gyr old) and fairly young ones (the bright blue plume). When simulated with the synthetic CMD method, this region appears to have experienced a mildly *gasping* (originally defined by Marconi et al. 1995) regime of SF over most of its

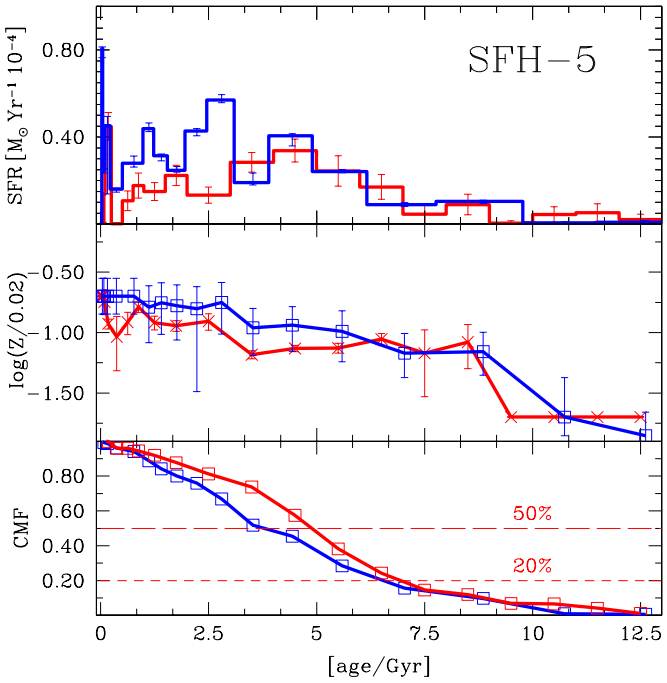

Figure 3. Recovered SFHs (top panel), AMRs (middle panel), and CMF (bottom panel) for SFH5 using the Bologna (SF5-B, red histogram) and Cole procedures (SFH5-C, blue histogram).

(A color version of this figure is available in the online journal.)

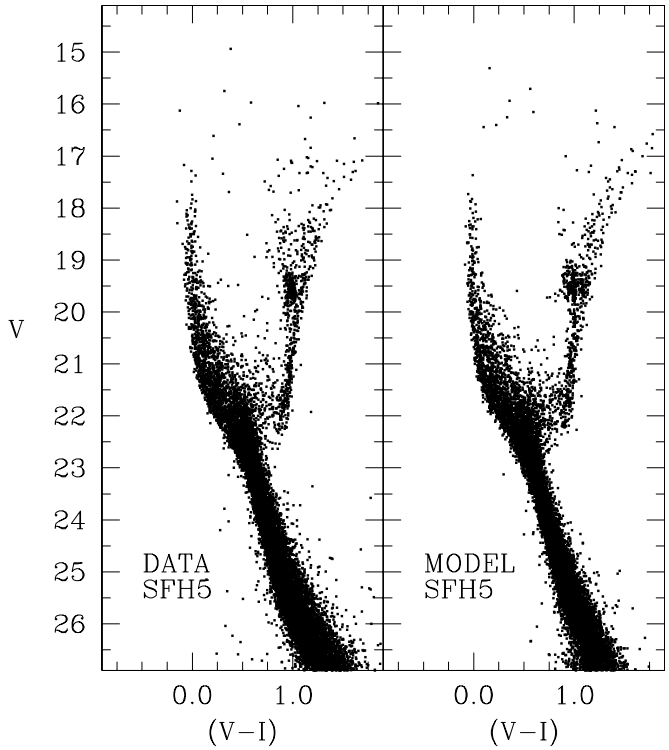

Figure 4. Comparison between the observational (left panel) and the Bologna synthetic CMD (right panel) for SFH5.

life, with peaks and dips of similar duration and rates within a factor of two of the average value. The top panel of Figure 3 shows SFH5's SFH as recovered using Bologna's (SFH5-B, red line) and Cole's procedures (SFH5-C, blue line).

Figure 4 shows the synthetic CMD (right panel) drawn from the Bologna SFH compared to the data (left panel). From a morphological point of view, the MS and the SGB are well reproduced, while the RC and Blue Loop region are, respectively, slightly broader and less populated than the observational ones.

As shown in Figure 3, the two solutions share the common characteristics of a significant discontinuity between the activity in the earliest 5–6 Gyr and the subsequent epochs. Stars were already being formed in the earliest phases, but at a very modest rate, significantly lower than at later times.

Overall, both solutions predict that (1) only 20% of the stellar mass was in place before 7.5 Gyr ago (see bottom panel of Figure 3, where the cumulative mass fraction, CMF, is plotted) and (2) the average SFH has not dropped significantly since its major event at 5 Gyr ago.

However, there are apparent differences between the two results. First, the degree of "burstiness" is higher in Cole's solution than in Bologna's. SFH5-C shows four SFR peaks a factor of two above the average: 4–5 Gyr ago (secondary peak), 2–3 Gyr ago (primary peak), 1 Gyr ago, and in the past 250 Myr, while SFH5-B shows a relatively smooth recent history, with only two peaks slightly above the average, at about 4.5 Gyr ago (primary peak) and 1.5–1.8 Gyr ago with gasps ≈0.4 and 1.2 Gyr. These differences can be partially explained by the higher age resolution adopted in Cole's approach. Second, the CMFs are slightly different in the range 2.5–5 Gyr ago, with SFH5-B reaching the 50% level about 1 Gyr before SFH5-C. This effect is likely due to a combination of several model inputs, including the adopted metallicity grid,[10] the CMD binning and interpretation (Bologna's approach attempts to fit the whole CMD, whilst Cole's approach restricts the analysis to MS and SGB stars), the general ability of each approach to escape from local minima, etc. Since these effects are strongly interlaced, we consider the differences in the solution as a measure of the systematic uncertainty.

To compare the performances of the two solutions, we plot in Figure 5, from left to right, the Hess diagram for the data (panels (a) and (d)), residuals (panel (b) for Cole, panel (e) for Bologna), best model CMDs (panel (c) for Cole and panel (f) for Bologna). From these diagrams it can be seen that both models show equally scattered residuals in the regions of the MS (above $I = 22$), SGB, and RGB, with no evident systematic departure (except for a vertical mismatch of Cole's model at $V - I \approx 0.6$). On the other hand, both models have shortcomings in reproducing details of the RC region: Cole's model predicts too many RC stars, but qualitatively reproduces the RC morphology; Bologna's model fits well the number of RC stars, but predicts a slightly different shape of the RC.

More subtle differences appear when one compares the luminosity functions (Figure 6) from our models with the observational ones. In the left panel (stars with $V - I < 0.6$), the Bologna model slightly underpredicts the number of MS stars in the magnitude range $20 < I < 21$, and both models overpredict the observed counts in the MS range $21.5 < I < 22$. In the right panel (stars with $V - I > 0.6$), Cole's model clearly overpopulates the RC (the peak around $I = 18.6$). The latter mismatch is a likely consequence of Cole's approach, which

[10] Although the two codes adopt the same Padova library, Bologna's code uses only the stellar tracks provided by Bertelli et al. (2008, 2009), whereas Cole's code also uses tracks with interpolated metallicities.

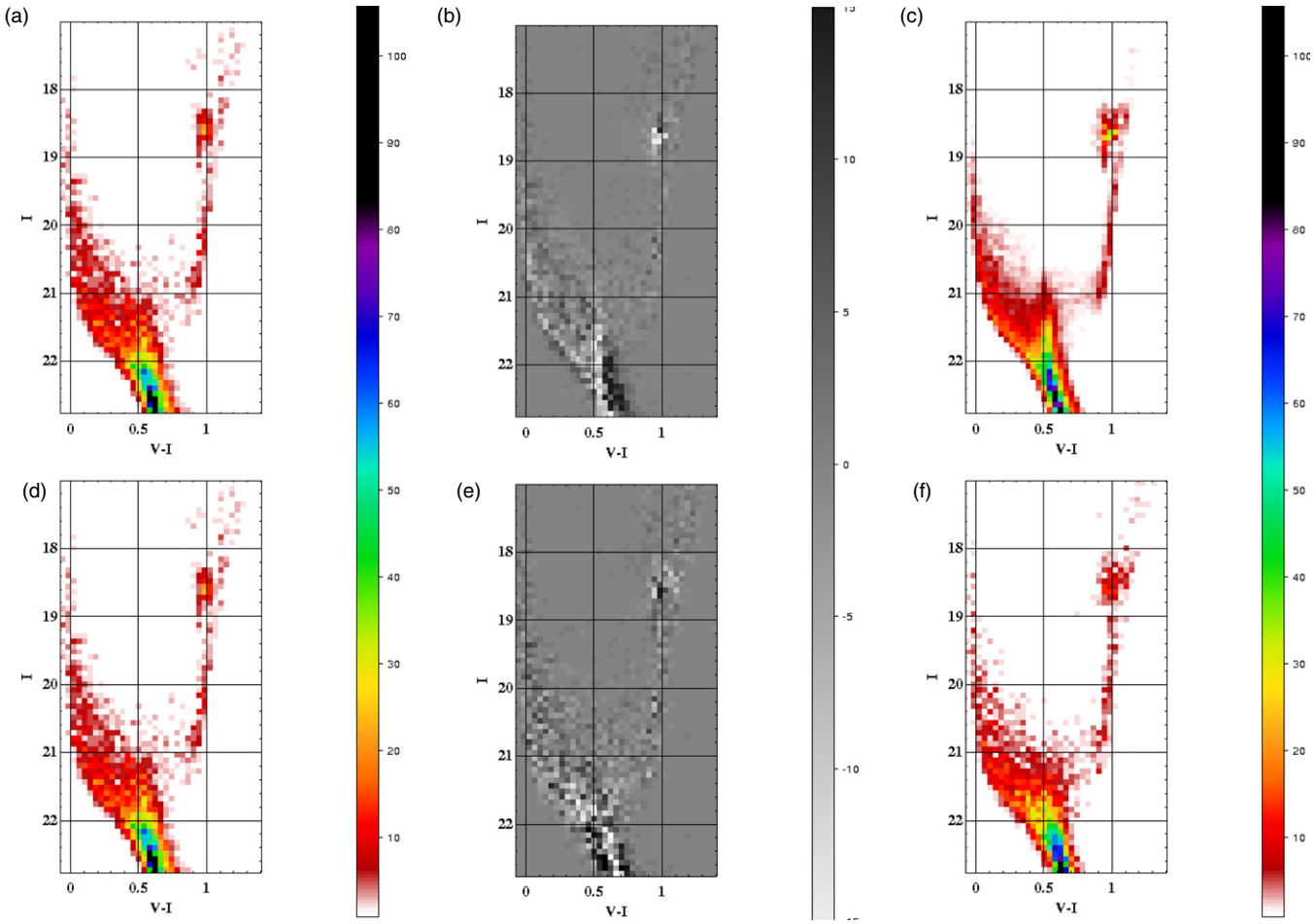

Figure 5. Comparison between observational and synthetic Hess diagrams for SFH5. Panels (a) and (d) show the data; panels (b) and (e) show the Cole and Bologna residuals (subtraction of the observed Hess diagram from the calculated one); and panels (c) and (f) show the Cole and Bologna best models, respectively.

(A color version of this figure is available in the online journal.)

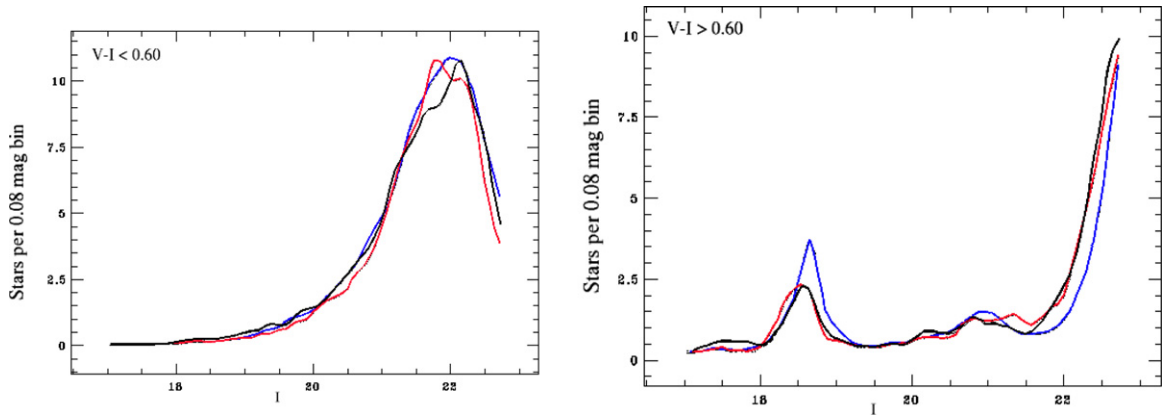

Figure 6. Comparison of the predicted and observational luminosity functions (I mag) for blue (left panel) and red (right panel) stars in SFH5. The blue lines correspond to Cole's best solutions, the red lines to Bologna's, and the black lines to the data.

(A color version of this figure is available in the online journal.)

uses only MS and SGB stars to recover the SFH, leaving RC and RGB regions unconstrained.

Concerning the recovered chemical history, Bologna's metallicity is slightly higher than Cole's prior to 7.5 Gyr ago, while the opposite is true at later times. However, the two results are consistent with each other within the uncertainties, also considering the coarser bin size (0.3 dex) of the Bologna metallicity network.

The differences between the Bologna and Cole solutions are the result of the assumptions of the codes and of the way in which the best-fit models are determined. The normalization over the past ≈5 Gyr (Cole's SFR is slightly higher than Bologna's) can, at least in part, be attributed to the different assumed IMFs, which diverge at 1 $M_{\odot}$, roughly the MSTO mass for a 5 Gyr age at SMC metallicities. The differences in bursty versus smooth SFH are likely the result of degeneracies

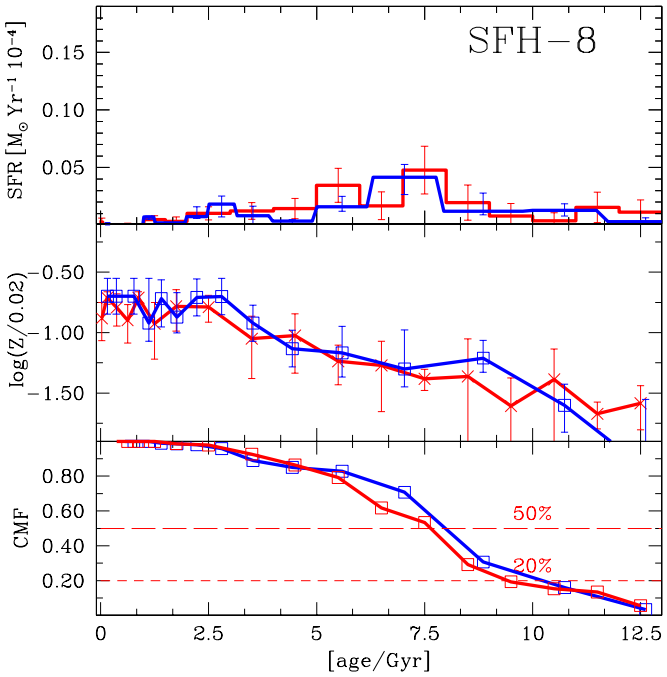

Figure 7. SFH, AMR, and CMF for SFH8. Colors and lines are as in Figure 3. (A color version of this figure is available in the online journal.)

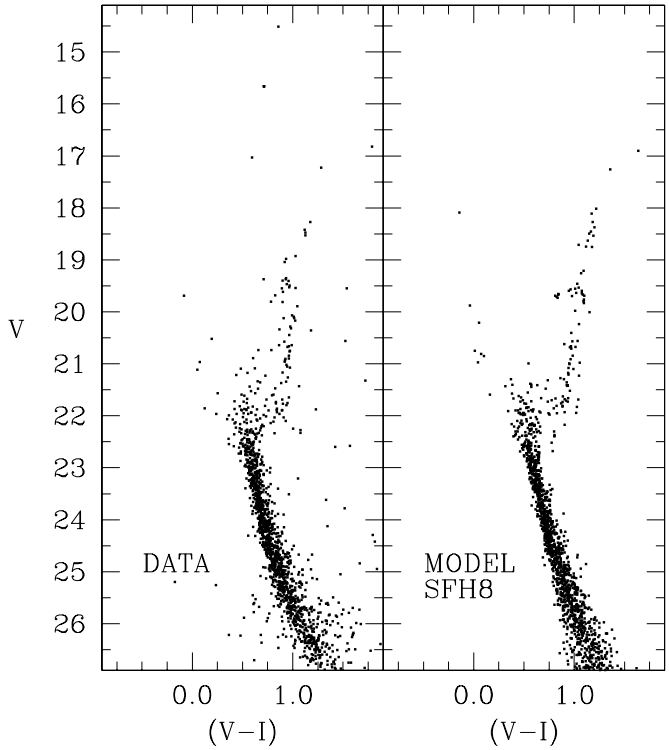

Figure 8. Comparison between the observational (left panel) and the Bologna synthetic (right panel) CMDs for SFH8.

between age, metallicity, distance, and reddening, and the way in which those degeneracies are broken given the adopted isochrones. Age–metallicity effects are suspected here owing to the divergence between the inferred AMRs from 1–3 Gyr ago, where the SFH differences are most pronounced.

Of the four fields analyzed in this paper, only SFH5 shows differences larger than the formal uncertainties on the solutions; it is no coincidence that this is the most crowded field, with the highest SFR, where differential reddening is also present. Similar effects were seen at a similar level in the bar fields analyzed in Cignoni et al. (2012).

The overall SFH in SFH5 is qualitatively similar to those of our bar fields SFH4 and SFH1 (see Cignoni et al. 2012); all three fields formed the majority of their stars in the past 5–6 Gyr. The very low rate of early SF (>10 Gyr ago) is consistent with the lack of a net HB in their CMDs. Additionally, the average SFR has been almost constant (SFH1) or slightly declining (SFH5 and SFH4) over the past few Gyr, although peaks and dips at various times and amplitudes are observed, as typical of gasping regimes.

3.2. SFH8

SFH8 is our most distant field in the SMC outer regions. Its CMD is characterized by the lack of a clear blue plume, as expected for a region sufficiently away from the star-forming body of the galaxy. Although it lies well within the density profile break taken to mark the transition to a "halo" (Nidever et al. 2011), it shows no evidence for recent star-forming activity. Both the solutions SFH8-B and SFH8-C (see top panel of Figure 7) find that the field has been quiescent since ∼1 Gyr. Both methods also agree on a rather moderate SF activity earlier than 7 Gyr ago, with the first (modest) SFR peak occurring between 5 and 9 Gyr ago. There was SF already taking place 13 Gyr ago, but at a very low rate. The activity in the past 3 Gyr is very low and concentrated in few episodes. Figure 8 shows the synthetic CMD (right panel) generated from the Bologna solution compared to the data (left panel). The turnoff (TO) region is well reproduced, as well as the MS, SGB, and lower RGB. The only visible differences are noted at the very bright end of the CMD ($14 < V < 17$), where a few objects are not matched by any simulation and are probably foreground stars, and at the very faint end (below $V = 25$), where our model overpredicts star counts.

Despite these similar rates and timings, Cole's and Bologna's AMR/CMF show some slight differences. As found for SFH5, Bologna's metallicity is systematically higher at early epochs (although still within the uncertainties). On the other hand, in the range 5–10 Gyr ago Cole's CMF generally rises faster than Bologna's.

There is also the possibility that the poorly populated upper MS in SFH8's CMD be contaminated (or dominated) by blue stragglers. It is well known that such objects populate dwarf spheroidals (see, e.g., Momany et al. 2007). Given the relatively low densities in those stellar systems, it is likely that their blue stragglers stem from primordial binary systems rather than from collisional binaries as in globular clusters. In this regard, we expect that genuine young MS stars are likely concentrated on the scale of the star-forming regions while blue stragglers are more widespread, presumably following the distribution of the bulk of stars in the SMC. Unfortunately, our field of view is small (∼60 pc) compared to the size of the SMC, so it is virtually impossible to distinguish any difference in the spatial distribution. Forthcoming wide-field observations with the VST will help elucidate this point.

3.3. SFH9

In spite of its large apparent distance from the galactic center and its low stellar density, SFH9 contains a significant fraction of young stars, as clearly indicated by the CMD blue plume.

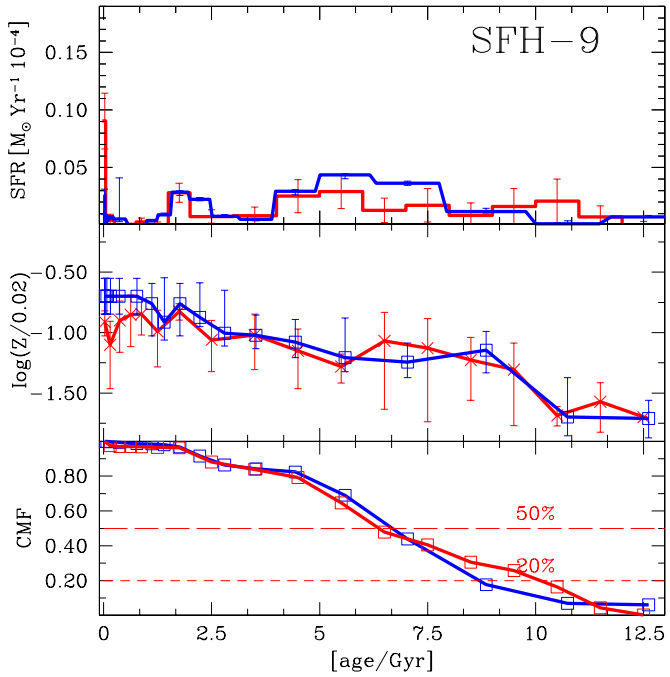

Figure 9. SFH, AMR, and CMF for SFH9. Colors and lines are as in Figure 3. (A color version of this figure is available in the online journal.)

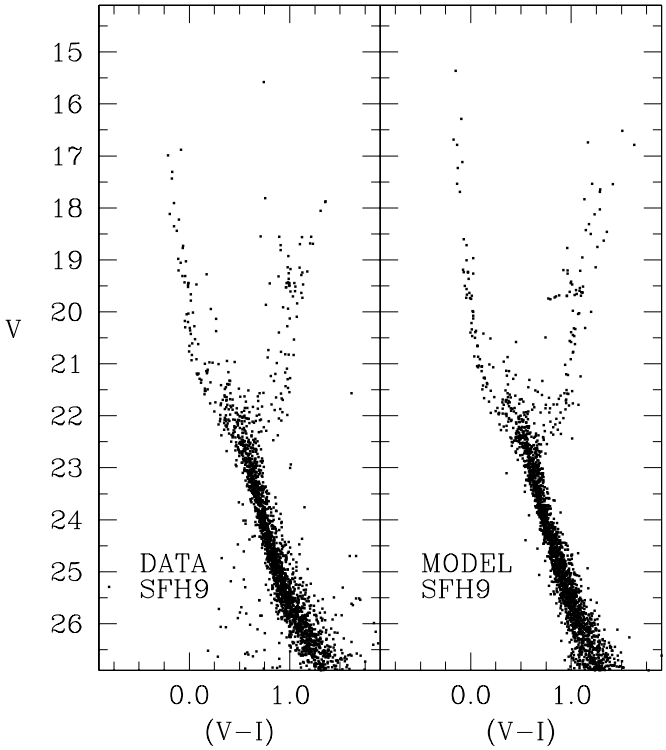

Figure 10. Comparison between the observational (left panel) and the Bologna synthetic (right panel) CMDs for SFH9.

This is robustly confirmed by our synthetic CMD analyses, which all show a significant enhancement in the SFR at very recent epochs (see the top panel in Figure 9). The only visible differences between the two solutions are the slightly higher activity of SFH9-C between 5 and 7.5 Gyr ago and the stronger peak of SFH9-B in the past 50 Myr. The corresponding AMRs are in very good agreement, except in the past 2 Gyr, where Cole's metallicity is slightly higher.

In both SFH9-B and SFH9-C, the average SFR has been quite low all over the Hubble time, not much different from that in SFH8, including the very modest peak around 5–6 Gyr ago and the almost quiescent initial phases. What makes this region different from SFH8 is the activity over the past ≈200 Myr. These stars have not had time to diffuse throughout the galaxy since their formation and remain close to their birthplace in the SMC wing.

Figure 10 shows the Bologna synthetic CMD (right panel) compared to the data (left panel). The overall agreement is excellent, with only minor differences in the RGB, which is sharper in the synthetic CMDs, and in the He-burning region, where our model predicts a mild HB instead of the observed round RC. It is also worth noting the apparent broadening of the lower MS, a feature which is not reproduced by our model. Likely explanations are (1) the fraction of binaries in the field SFH9 is larger than the adopted value (30%); (2) the metallicity of the youngest populations is higher than the expected value; and (3) a population of low-mass PMS (a stellar phase not included in these models) stars is present in the field. Since such MS splitting is not seen in SFH8, whose population is slightly older than but very similar to that of SFH9, we consider the first hypothesis unlikely.

3.4. SFH10

SFH10 lies midway between the bar and the wing, and its SFH is correspondingly intermediate between SFH5 and SFH9. Figure 11 shows the resulting SFHs according to the Bologna

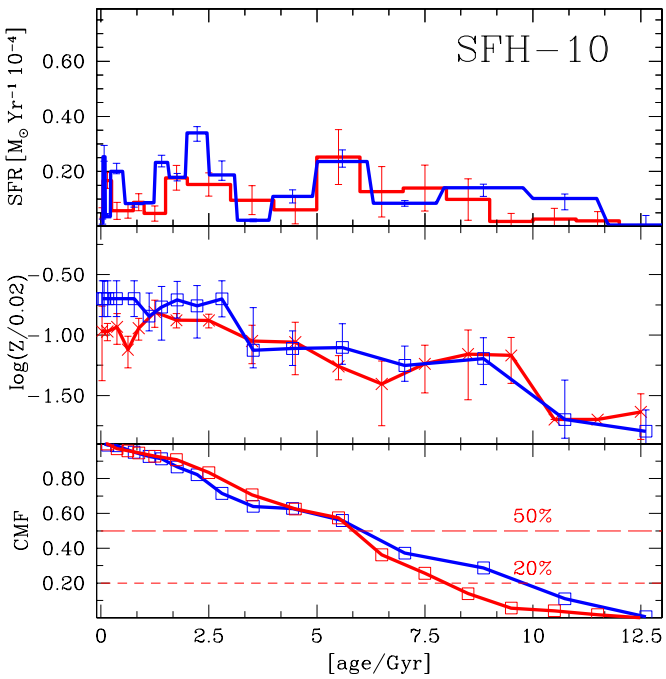

Figure 11. SFH, AMR, and CMF for SFH10. Colors and lines are as in Figure 3. (A color version of this figure is available in the online journal.)

and Cole approaches. SFH10-B and SFH10-C agree very well in predicting (1) a low activity in the first 5 Gyr; (2) a smooth increase from 8 to 5 Gyr ago; (3) a hiatus in SF from 3 to 4 Gyr ago; (4) an SF peak between 3 and 2 Gyr ago; and (5) a fairly smooth decrease since then, broken by a recent burst of SF. Both the AMRs and CMFs are in excellent agreement. The only difference here is the average rate of SFH10-C, which is slightly higher than SFH10-B.

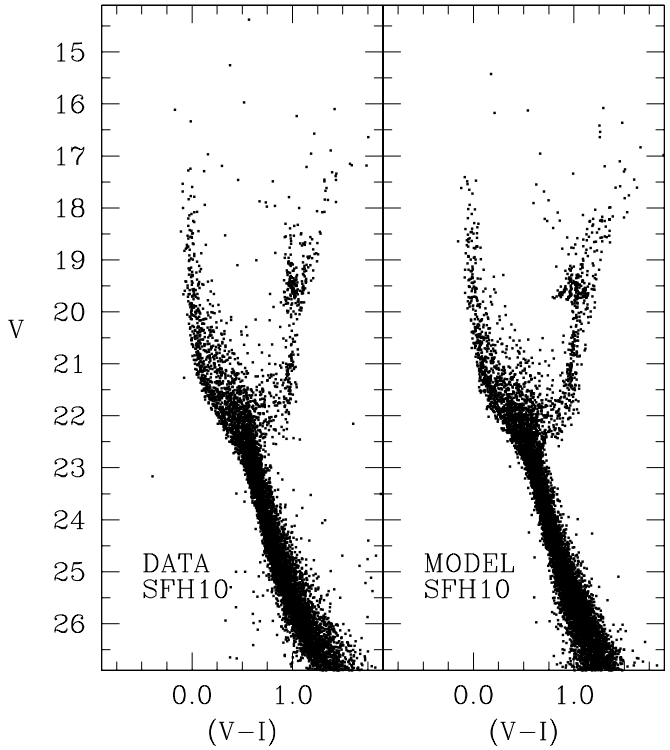

Figure 12. Comparison between the observational (left panel) and the Bologna synthetic (right panel) CMDs for SFH10.

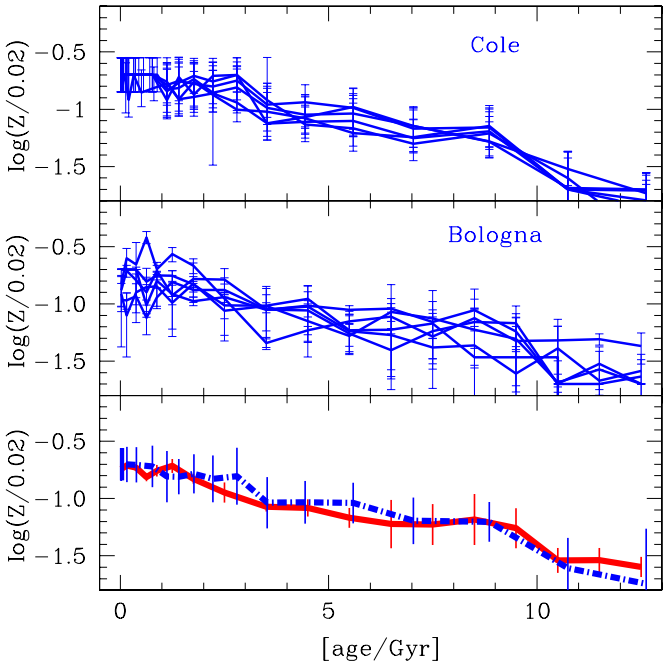

Figure 13. Top panel: Cole AMRs. Middle panel: Bologna AMRs. Bottom panel: average Bologna AMR (red solid line) vs. Cole (dot-dashed blue line) AMR.

(A color version of this figure is available in the online journal.)

The comparison between the SFH9 and SFH10 histories shows intriguing similarities and differences. First of all, the global morphology of their SFHs is rather similar, although SFH10 has experienced a much more intense SF activity for most of the time. However, in spite of the globally higher rate, the activity of SFH10 in the past 50 Myr is lower than in SFH9. This means that SFH9 has been forming stars at a slower pace than SFH10 for most of its life, as expected for its larger distance from the SMC center, but has suddenly undergone a significant SF enhancement that has made it currently much more active than SFH10. This strongly suggests that the ongoing SF in SFH9 is not motivated by the typical gas density in the SMC periphery, but has been stimulated by some external process. If we add the evidence that SFH9 lies in the wing region characterized by a string of H II regions that extend into the Magellanic Bridge, one is driven to conclude that the interaction with the LMC is the main culprit.

Figure 12 shows the Bologna synthetic CMD (right panel) compared to the SFH10 data (left panel). Also for this field the model fits very well the observations. Few minor mismatches remain in the shape of the RC, which is slightly broader in the model.

3.5. Age–Metallicity Relation: a Global View

In spite of the uncertainties, our AMRs portray a consistent picture of a metallicity increasing with time. Figure 13 shows a composite plot with all our six AMRs (including our solutions for SFH1 and SFH4; see Cignoni et al. 2012). The top and middle panels summarize the Cole and Bologna solutions for each field, while the bottom panel compares the average Bologna (red line) and Cole (blue line) AMRs.

By comparing the results of the two methods, we can conclude that (1) within the uncertainties our solutions are consistent in all fields and (2) the SMC experienced a very slow metallicity evolution until around 2 Gyr ago and a steeper enrichment since then.

There are also few systematic differences that are worth discussing. At early times, the mean metallicity of Bologna solutions is higher than Cole's, while at intermediate ages, it is generally lower. Moreover, the Bologna solutions show a higher dispersion. All these variations are mostly due to differences in the metallicity grid adopted in the two methods. Given the coarser metallicity resolution of the Bologna set of stellar models, and because of the degeneracy between reddening and metallicity, a small variation of the adopted reddening may result in a quite different average metallicity (up to 0.3 dex). This effect is necessarily exacerbated in those fields which are dominated by an old population. Moreover, the lowest metallicity of the Bologna set of stellar models ($Z = 0.0004$) is higher than the corresponding one of Cole's set ($Z = 0.00015$): this naturally explains the lower metallicity predicted at early times by Cole's method.

4. COMPARISON WITH OTHER STUDIES

4.1. SFHs

Our results confirm that most of the central SMC regions have had very little SF activity in the first few billion years of galaxy life, as already found by several authors (Dolphin et al. 2001; McCumber et al. 2005; Chiosi & Vallenari 2007; Cignoni et al. 2012; Weisz et al. 2013). Further support to this conclusion is provided by the relatively low number of RR Lyrae stars detected in the SMC compared to the LMC (Soszyñski et al. 2010) and by the circumstance that the SMC oldest cluster, NGC 121, is only 11 ± 0.5 Gyr old (Glatt et al. 2008a), i.e., much younger than the oldest globular clusters hosted in the Galaxy and in the LMC.

Noël et al. (2007) also found that a shared feature of all their 12 SMC fields is the absence of a well-populated, blue, extended

HB, pointing out that the number of field stellar populations as old and metal-poor as that of the Milky Way (MW) halo globular clusters and dwarf spheroidal galaxies is small in the SMC. However, in their subsequent synthetic CMD analysis, Noël et al. (2009) suggested that significant SF activity also took place at the earliest epochs, with a sizable difference between the eastern and western fields.

Harris & Zaritsky (2004), who were the first to apply the synthetic CMD method to the derivation of the SMC SFH, suggested that 50% of SMC stars formed earlier than 8.4 Gyr ago, and that very few formed in the period between 3 and 8.4 Gyr ago. However, contrary to all the subsequent quoted studies, their ground-based photometry did not reach the oldest MSTO, and this hampered the derivation of the SFH at relatively early epochs. This points to the importance of high angular resolution in minimizing the effect of crowding on deep CMD analyses. We will be able to further quantify the SF level at the earliest epochs over the full extent of the SMC when the VST Guaranteed Time Observations are completed, but these must still be tied to diffraction-limited imaging studies where the stellar density is high.

All our fields experienced their first significant SF activity around 8–10 Gyr ago, which reached a peak a few Gyr later. This behavior is shared also by the fields studied by Dolphin et al. (2001), McCumber et al. (2005), Chiosi & Vallenari (2007), and Noël et al. (2007; 2009).

As displayed by Cignoni et al. (2012) in their Figure 1, our examined regions lie close to some of those analyzed by other authors, and it is interesting to compare our results with theirs.

Our field SFH8 in the northern outskirts of the galaxy is rather close to those studied by Dolphin et al. (2001), who concluded that stars in the outskirts of the SMC formed during a broadly peaked episode of SF, with the largest (although moderate) rate between 5 and 8 Gyr ago. We find exactly the same result. SFH8 is also not too distant from the field qj0033 studied by Noël et al. (2009), who derived for it an SFH consistent with ours, with two moderate activity peaks 5 and 8 Gyr ago. The only significant difference is before 10 Gyr ago, where Noël's (2009) activity is higher than in our solutions. However, most of the information at these epochs is conveyed by the oldest TOs, which are much better defined in our data. Weisz et al. (2013) also studied a region near our SFH8, reanalyzing WFPC2 fields (their fields 4–7). They find a similar truncation of major SF at ages ≈3–5 Gyr, with a median formation age of ≈7 Gyr, identical to our result within the errors.

On the opposite side of the SMC, our SFH9 region is the most external field studied so far with ACS. The closest field available in the literature with SFH inferred from the CMD is qj0116 of Noël et al. (2009), located halfway between our SFH9 and SFH10 regions, and the two analyses are in excellent agreement. In SFH9, we find moderate SF activity, characterized by a very recent burst, a moderate peak around 5–6 Gyr ago, and very low rates in the first 4 Gyr. In qj0116, Noël et al. (2009) also found that the most significant star-forming activity was in the past 1 Gyr, preceded by a more modest rate over most of the Hubble time, with a secondary peak 5 Gyr ago and a very low initial rate.

Our intermediate field SFH10 lies close to the field studied by McCumber et al. (2005) and the three fields analyzed by Noël et al. (2009); in particular, SFH10 is near their qj0111 field. Our analysis shows that SFH10 has had a fairly continuous SFH in the past 8–9 Gyr, after the usual enhancement over the very modest initial activity. This is only partially consistent with McCumber et al. (2005), who found for their region an increasing rate from 12 to 4 Gyr ago and over the past 1.5 Gyr, with a significantly quieter phase between 4 and 1.7 Gyr ago. Noël et al. (2009) found in qj0111 a highly variable SFH, with a first secondary SF peak 10 Gyr ago followed by a dip 3 Gyr later, a primary peak about 4 Gyr ago followed by a similar dip 2 Gyr ago, and a new recent peak. Although a similar "gasping" behavior is also found in our solution, the timing of the peaks is different and the earliest activity is higher than ours. In conclusion, none of the three studies are in good agreement with the other two.

SFH5 is not coincident with any field with SFH derived from the CMD, except of course those by Harris & Zaritsky (2004) that cover the whole SMC but suffer from poor completeness affecting the SFR measurements for ages older than a few Gyr. Of the fields with photometry reaching the old MSTO, smc0057 of Noël et al. (2009) is not too distant, and field SMC-1 of Weisz et al. (2013) is nearly midway between our SFH1 and SFH5. For smc0057, Noël et al. (2009) suggest a bouncing SFH not too different from what we find for SFH5, except that in our field we have a significant recent burst which is absent in their field, probably because theirs is slightly more external and away from the star-forming regions. Another interesting difference is that also in this region we find only a very moderate initial activity, while smc0057 shows a primary peak 12 Gyr ago.

Weisz et al. (2013) find evidence for a burst of SF ∼9 Gyr ago in their field SMC-1, with a long period of low SFR punctuated by a minor episode at 5 Gyr and then a dramatic and sustained increase at ∼3 Gyr. In this respect, the Weisz et al. (2013) solution is a more extreme version of our Cole solution, sharing the same median age of formation with that solution (Figure 3). The reason for the differing SFR at old age is not obvious, as the WFPC2 completeness levels are not dramatically shallower than the ACS levels; however, it is worth noting that over the time period from ∼7 to 13 Gyr ago, the error bars on the CMF shown by Weisz et al. (2013) are skewed to the low side, suggesting that the significance of the increase in SFR at 9 Gyr is low.

Finally, we recall that our SFH1 region, described by Cignoni et al. (2012), almost coincides with two of the three deep bar fields studied by Chiosi & Vallenari (2007) around the SMC clusters K29, NGC 290, and NGC 265, as well as SMC-2 and SMC-3 from Weisz et al. (2013). Our and their solutions are in good qualitative and quantitative agreement and show an unambiguous rise of the SFR between 7 and 5 Gyr ago and a very moderate earlier activity. However, Weisz et al. (2013) tend to find that the 20% level in the CMF is reached earlier and the 50% level is reached later than in our solutions.

4.2. AMRs

4.2.1. Field Star AMR

Concerning the field AMR, Figure 14 shows Bologna and Cole solutions[11] along with the most comprehensive field AMR studies, namely, Piatti (2012a, hereinafter P12, yellow filled circles) and Carrera et al. (2008, hereinafter C08, magenta filled triangles). These works are independent and spatially complementary: the former derived a global AMR using Washington photometry for 160 9×9 arcmin^2 regions across the SMC main body, while the latter used Ca II triplet spectroscopy for 13 regions in the SMC outskirts. Overall our solutions

[11] To convert from Z metallicities to [Fe/H] values, we adopted $Z_\odot = 0.02$ and $[\mathrm{Fe/H}] = \log(Z/Z_\odot)$.

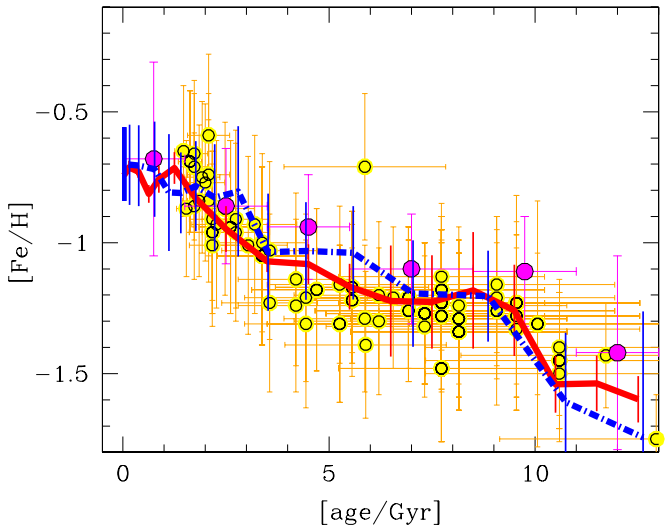

Figure 14. Comparison of our predicted average AMRs with literature data for SMC field stars. Solid red line: average Bologna AMR. Blue dot-dashed line: average Cole AMR. Yellow filled circles: mean ages and photometric metallicities of selected fields in the SMC derived by Piatti (2012a). Each point represents an SMC sector of about 9×9 arcmin^2. Magenta filled circles: Ca II triplet AMR derived by Carrera et al. (2008).

(A color version of this figure is available in the online journal.)

compare favorably with both P12 and C08 data,[12] at a level largely consistent with the uncertainties. The agreement is better when the metallicity is high, while some differences appear below [Fe/H] $= -1$. In particular, our AMRs are at the upper edge of P12 distribution between 4 and 6 Gyr ago, while they are at its lower edge prior to 9 Gyr ago. Conversely, both the Bologna and Cole AMRs are systematically metal poorer than that of C08 prior to 5 Gyr ago, although always within the error bars.

Taken at face value, these findings might suggest that our *HST* fields experienced a chemical enrichment at early times slower than in the rest of the SMC. The situation is less clear at intermediate ages where P12 and C08 data enclose our solutions. However, it should be stressed that the large uncertainties in the ages of both P12 and C08 data sets can contribute to flatten their AMR, e.g., producing more relatively metal-rich old stars.

4.2.2. Star Cluster AMR

Figure 15 shows the comparison with cluster ages and metallicities collected from the literature. Specifically, small filled triangles are photometric determinations (Piatti et al. 2001, 2005, 2007, 2011; Piatti 2011a, 2011b, 2012b; Mighell et al. 1998; Sabbi et al. 2007), while large filled triangles are spectroscopic determinations (Da Costa & Hatzidimitriou 1998;[13] Glatt et al. 2008a, 2008b; Parisi et al. 2009).

Despite the large scatter at any given age and also considering the large uncertainties, our AMRs are in reasonable agreement with the cluster AMR. Indeed, it is noteworthy that the Glatt et al. (2008a, 2008b) clusters (filled red triangles), whose ages have been determined from deep *HST* CMDs and spectroscopic metallicities, are those providing the best match to our AMRs (with the exception of Lindsay 38). Actually, a close inspection suggests that a large fraction of the cluster symbols are located *below* our AMRs. As pointed out by Glatt et al. (2008b), at any given age the SMC clusters show a range of metallicities that exceeds the spectroscopic uncertainties, indicating that the SMC was not well mixed.

[12] We point out that the quoted [Fe/H] literature values probably adopt different $\log(\mathrm{Fe/H})_\odot$ not always given in the papers.

[13] Lindsay 1, Kron 3, and NGC 121 were not included because ages were updated by Glatt et al. (2008a, 2008b).

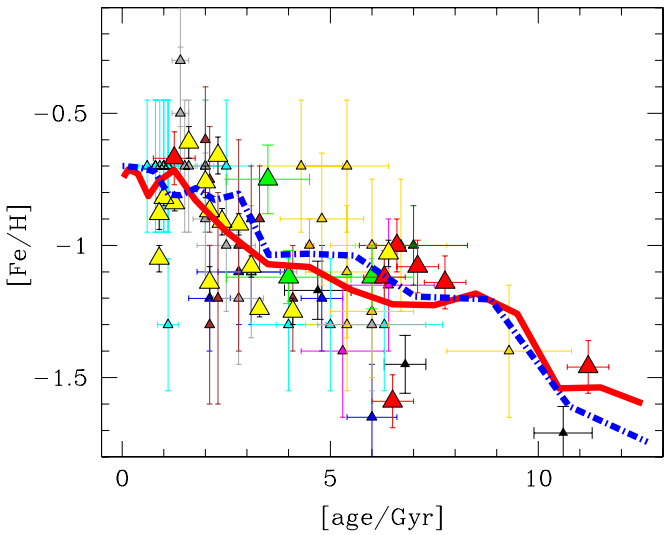

Figure 15. Comparison of our predicted average AMRs (same symbols as in Figure 14, theoretical error bars have been omitted for clarity) with literature data for SMC clusters. Small and large triangles represent photometric and spectroscopic (Ca II triplet) determinations, respectively: Da Costa & Hatzidimitriou (1998, light green filled triangles), Glatt et al. (2008a, 2008b, red filled triangles), Parisi et al. (2009, yellow filled triangles), Mighell et al. (1998, black filled triangles), Sabbi et al. (2007, orange filled triangles), Piatti et al. (2001, blue filled triangles), Piatti et al. (2007, magenta filled triangles), Piatti et al. (2011, cyan filled triangles), Piatti (2011a, dark yellow filled triangles), Piatti (2012b, dark green filled triangles), Piatti (2011b, gray filled triangles), and Piatti et al. (2005, brown filled triangles).

(A color version of this figure is available in the online journal.)

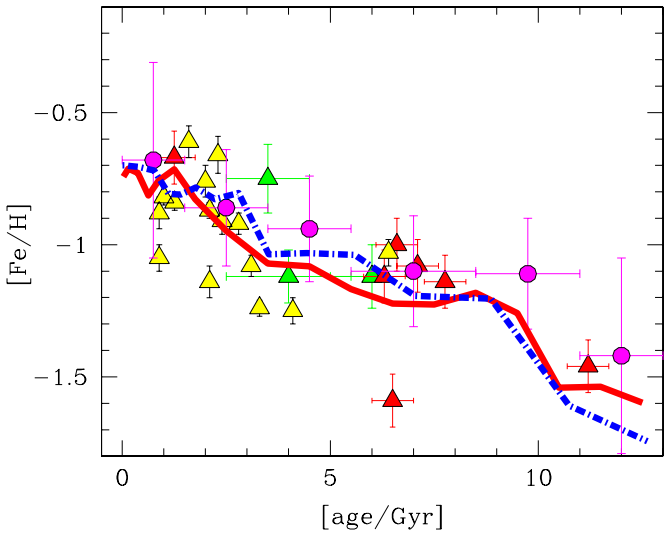

Figure 16. Comparison of our predicted average AMRs (same symbols as in Figure 14, theoretical error bars have been omitted for clarity) with literature spectroscopic data only (cluster and field stars): Da Costa & Hatzidimitriou (1998, green filled triangles), Glatt et al. (2008a, 2008b, red filled triangles), Parisi et al. (2009, yellow filled triangles), and C08 (magenta filled circles).

(A color version of this figure is available in the online journal.)

4.2.3. Spectroscopic AMR

Figure 16 shows the comparison between our AMRs and all available spectroscopic derivations, regardless of whether measured in clusters or in the field. We point out that the general

agreement is improved (in particular between 1 and 9 Gyr ago), with our predictions within most of observational uncertainties. This suggests that, when accurate metallicity measurements are taken into account, cluster and field AMRs may be consistent with each other.

5. SUMMARY AND DISCUSSION

We can summarize our results as follows.

1. All six SFHs show that the SMC experienced a global peak of SF between 4 and 7 Gyr ago. The onset time of this event is consistent across all fields, while the amplitude strongly varies. There is some evidence that the duration of the global peak is longer in the inner fields, although the degree to which this is a continuous process as opposed to a discrete series of shorter events cannot be unambiguously assessed with the current data.

   This result is consistent with the sudden appearance of the relative excess of clusters found by Piatti (2011b) around 7–8 Gyr ago. From a theoretical point of view, this enhancement poses a serious challenge to current dynamical models if we assume that cluster formation and field SF are primarily interaction triggered. Besla et al. (2012) predict that the LMC and the SMC are a pair of tidally interacting galaxies that have recently been accreted by the MW, while Diaz & Bekki (2011) argue that around 5.5 Gyr ago the LMC and SMC were isolated (200 kpc from each other). So how can we explain the relatively old SF onset in terms of mutual interactions of SMC/LMC/MW?

   An intriguing and alternative scenario is the one proposed by Tsujimoto & Bekki (2009): a major merger event took place 7.5 Gyr ago in a small group environment that was far from the MW and contained a number of small gas-rich dwarfs comparable to the SMC. Although attractive, their model also predicts a dip in the SMC AMR (due to the large gas infall during the merging), which is in contrast with our solutions showing flat or slightly increasing profiles. However, a minor merger, which would produce a small dip, may be still a viable possibility.

   It should be kept in mind that major interactions are not needed for small galaxies to experience a sudden increase in SFR following a long period of inactivity—examples include IC 1613 (Skillman et al. 2003), DDO 210 (McConnachie et al. 2006), Leo A (Cole et al. 2007), IC 10 (Hunter 2001; Cole 2010), and NGC 6822 (Cannon et al. 2012). The latter two are of very similar total mass to the SMC, and while they are both undergoing a current episode of interaction-triggered SF, they have similar mean ages to the SMC and no obvious counterpart for a major interaction. This may be a hint that SMC-mass galaxies are capable of large excursions in mean SFR without major mergers or interactions.
2. The sequence of fields SFH1, SFH5, SFH4, SFH10, SFH9, and SFH8 represents a sequence of age from the youngest (SFH1) to the oldest (SFH8). This general trend reflects well the distribution of star clusters (see Figure 7 in Glatt et al. 2010).

   All fields share the common characteristics of having formed less than 20% of their mass prior to 10 Gyr ago. The median age rises from ≈4 to ≈6 Gyr as the projected distance increases from 0.05 to 2.2 kpc, largely owing to the decreasing amplitude of the intermediate-age SFR enhancement that dominates the bar fields. The entire CMF appears to be shifted to older ages in the outer fields, with the 20th percentile of stellar mass in place by ≈9.5 Gyr in the fields at ∼2.3 kpc, but not until ∼5–6 Gyr in the bar. The bar fields are indistinguishable from the central fields off the bar at the same radius over virtually their entire lifetime, confirming that the bar is largely a "Population I" feature (see, e.g., Westerlund 1997; Zaritsky et al. 2000).
3. Field SFH9 shows the most peculiar SFH. It is located ∼2.3 kpc from the SMC center, at the same radial distance as the extremely quiet field SFH8, but on the side of the SMC closest to the LMC, in the wing of the SMC. This region is known for its disturbed H I morphology and young stellar populations. Indeed, we find that SFH8 and SFH9 have indistinguishable SFH for ages older than ≈1 Gyr, with a generally low SFR that shows significant activity only for ages older than ∼2.5 Gyr. However, the SFH9 region hosts a population younger than ∼200 Myr that is completely absent in SFH8. Such a population is also far weaker in the SFH10 field, which is at a similar position angle but midway between the wing and the bar. The shape of the upper MS in SFH9 is consistent with all of the bright stars having been formed in a single event, as the MS is extremely narrow and shows little evidence for a continuous distribution of MSTOs as exemplified by, e.g., SFH5.

   These findings support two mechanisms of SF: a spontaneous mode which depends on the density of cold gas available to form stars and a triggered mode induced by the LMC/MW gravitational wells. The first scenario can explain the progressively lower activity moving away from the SMC center where the gas supply was plausibly higher. In the second scenario, the young stellar populations in the wing field SFH9 are likely generated from gas pulled out from the SMC during a recent collision with the LMC. As a result, the recent activity in SFH10 is probably driven by a combination of factors, a relatively high gas supply (SFH10 is not much further away than SFH5) and the LMC compression, while the activity in SFH9, which is located far away from the SMC center, may be totally triggered, producing the strong contrast with the total lack of activity in the SFH8 field located at similar distance but on the anti-LMC side of the galaxy.
4. Our six AMRs are consistent with each other and taken as a whole are consistent with a fast initial enrichment prior to 9 Gyr ago, very slow metallicity evolution from ≈4–9 Gyr ago, and a second epoch of major enrichment at more recent times. This is in agreement with previous photometric (P12) and spectroscopic (C08) studies.

   Our six SFHs do not show evidence for a steep metallicity gradient in the SMC. However, the concentration of younger stars toward the inner regions combined with the AMR could be consistent with an apparent shallow metallicity gradient. Since the metallicity increases with time and the mean age increases with radius, the typical star at large radius is expected to be more metal-poor than the typical star at small radius. However, our CMDs indicate that at a given age there is very little difference in mean metallicity as a function of radius, a result largely borne out by spectroscopy of age-selected stellar tracers (see Westerlund 1997, Chapter 11, and references therein).

   Previous searches for spatial gradients have produced contrasting results. The spatial segregation of young and old stars was noted by Gardiner & Hatzidimitriou (1992) among others. Recently, Nidever et al. (2011) have detected

a 6 Gyr old relatively metal-poor population extending out to 8° in radius, while the younger stars (for example, carbon stars; Morgan & Hatzidimitriou 1995) are largely contained within 4° of the center. Among the stars and clusters older than 1 Gyr, there appears to be considerable scatter in metallicity, which tends to obscure trends by increasing the shot noise in typical samples. Among recent spectroscopic studies, there are significant differences in the reported field star metallicity trend with radius from 0° to 6°, including virtually no trend (Parisi et al. 2010), a steep gradient of $\lesssim$0.2 dex deg^{-1} (C08), and spatially segregated components at −0.6 (inner) and −1.25 (outer; De Propris et al. 2010). Photometric studies of field stars (e.g., P12) detect metal-rich stars concentrated toward the central regions but little to no evidence for gradients among the older stars. Although it is generally agreed that the younger populations concentrate toward the central regions, the degree of concentration, the characteristic ages of the inner and outer populations, and the steepness of the AMR over the relevant timescales are matters of continued discussion.

M.C. and M.T. have been partially funded with contracts COFIS ASI-INAF I/016/07/0, ASI-INAF I/009/10/0, and PRIN-MIUR 2010 LY5N2T. E.K.G. acknowledges partial funding from Sonderforschungsbereich "The Milky Way System" (SFB 881) of the German Research Foundation (DFG), especially via subproject A2. Partial support for J.S.G.'s analysis of data from *HST* program GO-10396 was provided by NASA through a grant from the Space Telescope Science Institute, which is operated by the Association of Universities for Research in Astronomy, Inc., under NASA contract NAS 5-26555.

REFERENCES

Anderson, J., & King, I. R. 2006, PSFs, Photometry, and Astronomy for the ACS/WFC (Instrum. Sci. Rep. ACS 2006-01; Baltimore, MD: STScI)
Anderson, J., Sarajedini, A., Bedin, L., et al. 2008, AJ, 135, 2055
Angeretti, L., Tosi, M., Greggio, L., et al. 2005, AJ, 129, 2203
Bertelli, G., Girardi, L., Marigo, P., & Nasi, E. 2008, A&A, 484, 815
Bertelli, G., Nasi, E., Girardi, L., & Marigo, P. 2009, A&A, 508, 355
Besla, G., Kallivayalil, N., Hernquist, L., et al. 2012, MNRAS, 421, 2109
Bothun, G. D., & Thompson, I. B. 1988, AJ, 96, 877
Cannon, J. M., O'Leary, E. M., Weisz, D. R., et al. 2012, ApJ, 747, 122
Carlson, L. R., Sabbi, E., Sirianni, M., et al. 2007, ApJL, 665, L109
Carrera, R., Gallart, C., Hardy, E., Aparicio, A., & Zinn, R. 2008, AJ, 135, 836
Cash, W. 1979, ApJ, 228, 939
Chabrier, G. 2003, PASP, 115, 763
Chiosi, E., & Vallenari, A. 2007, A&A, 466, 165
Cignoni, M. 2006, PhD thesis, University of Pisa
Cignoni, M., Cole, A. A., Tosi, M., et al. 2012, ApJ, 754, 130
Cignoni, M., Degl'Innocenti, S., Prada Moroni, P., & Shore, S. N. 2006, A&A, 459, 783
Cignoni, M., Sabbi, E., Nota, A., et al. 2009, AJ, 137, 3668
Cignoni, M., & Tosi, M. 2010, AdAst, 2010, 158568
Cignoni, M., Tosi, M., Sabbi, E., et al. 2010, ApJL, 712, L63
Cignoni, M., Tosi, M., Sabbi, E., Nota, A., & Gallagher, J. S. 2011, AJ, 141, 31
Cole, A. A. 2010, PASA, 27, 234
Cole, A. A., Skillman, E. D., Tolstoy, E., et al. 2007, ApJL, 659, L17
Crowl, H. H., Sarajedini, A., Piatti, A. E., et al. 2001, AJ, 122, 220
Da Costa, G. S., & Hatzidimitriou, D. 1998, AJ, 115, 1934
De Propris, R., Rich, R. M., Mallery, R. C., & Howard, C. D. 2010, ApJL, 714, L249
Diaz, J., & Bekki, K. 2011, MNRAS, 413, 2015
Dolphin, A. E., Walker, A. R., Hodge, P. W., et al. 2001, ApJ, 562, 303
Gardiner, L. T., & Hatzidimitriou, D. 1992, MNRAS, 257, 195
Glatt, K., Gallagher, J. S., III, Grebel, E. K., et al. 2008a, AJ, 135, 1106
Glatt, K., Grebel, E. K., Jordi, K., et al. 2011, AJ, 142, 36
Glatt, K., Grebel, E. K., & Koch, A. 2010, A&A, 517, A50
Glatt, K., Grebel, E. K., Sabbi, E., et al. 2008b, AJ, 136, 1703
Gonidakis, I., Livanou, E., Kontizas, E., et al. 2009, A&A, 496, 375
Greggio, L., Tosi, M., Clampin, M., et al. 1998, AJ, 504, 725
Harris, J., & Zaritsky, D. 2004, AJ, 127, 1531
Haschke, R., Grebel, E. K., & Duffau, S. 2011, AJ, 141, 158
Haschke, R., Grebel, E. K., Duffau, S., & Jin, S. 2012, AJ, 143, 48
Hunter, D. A. 2001, ApJ, 559, 225
Kapakos, E., Hatzidimitriou, D., & Soszyński, I. 2011, MNRAS, 415, 1366
Kroupa, P. 2001, MNRAS, 322, 231
Marconi, G., Tosi, M., Greggio, L., & Focardi, P. 1995, AJ, 109, 173
Mateo, M. L. 1998, ARA&A, 36, 435
McConnachie, A. W., Arimoto, N., Irwin, M., & Tolstoy, E. 2006, MNRAS, 373, 715
McCumber, M. P., Garnett, D. R., & Dufour, R. J. 2005, AJ, 130, 1083
Mighell, K. J., Sarajedini, A., & French, R. S. 1998, AJ, 116, 2395
Momany, Y., Held, E. V., Saviane, I., et al. 2007, A&A, 468, 973
Morgan, D. H., & Hatzidimitriou, D. 1995, A&AS, 113, 539
Nidever, D. L., Majewski, S. R., Muñoz, R. R., et al. 2011, ApJL, 733, L10
Noël, N. E. D., Aparicio, A., Gallart, C., et al. 2009, ApJ, 705, 1260
Noël, N. E. D., Gallart, C., Costa, E., & Méndez, R. A. 2007, AJ, 133, 2037
North, P., Gauderon, R., Barblan, F., & Royer, F. 2010, A&A, 520, A74
Nota, A., Sirianni, M., Sabbi, E., et al. 2006, ApJL, 640, L29
Parisi, M. C., Geisler, D., Grocholski, A. J., Claría, J. J., & Sarajedini, A. 2010, AJ, 139, 1168
Parisi, M. C., Grocholski, A. J., Geisler, D., Sarajedini, A., & Claría, J. J. 2009, AJ, 138, 517
Piatti, A. E. 2011a, MNRAS, 416, L89
Piatti, A. E. 2011b, MNRAS, 418, L69
Piatti, A. E. 2012a, MNRAS, 422, 1109
Piatti, A. E. 2012b, ApJL, 756, L32
Piatti, A. E., Clariá, J. J., Bica, E., et al. 2011, MNRAS, 417, 1559
Piatti, A. E., Santos, J. F. C., Clariá, J. J., et al. 2001, MNRAS, 325, 792
Piatti, A. E., Sarajedini, A., Geisler, D., Gallart, C., & Wischnjewsky, M. 2007, MNRAS, 381, L84
Piatti, A. E., Sarajedini, A., Geisler, D., Seguel, J., & Clark, D. 2005, MNRAS, 358, 1215
Ripepi, V., Marconi, M., Musella, I., et al. 2006, MmSAI, 9, 267
Sabbi, E., Gallagher, J. S., Tosi, M., et al. 2009, ApJ, 703, 721
Sabbi, E., Sirianni, M., Nota, A., et al. 2007, AJ, 133, 44
Schlegel, D. J., Finkbeiner, D. P., & Davis, M. 1998, ApJ, 500, 525
Sirianni, M., Jee, M. J., Benítez, N., et al. 2005, PASP, 117, 1049
Skillman, E. D., Tolstoy, E., Cole, A. A., et al. 2003, ApJ, 596, 253
Soszyński, I., Udalski, A., Szymański, M. K., et al. 2010, AcA, 60, 165
Subramanian, S., & Subramaniam, A. 2009, A&A, 496, 399
Tolstoy, E., Hill, V., & Tosi, M. 2009, ARA&A, 47, 371
Tosi, M., Gallagher, J. S., III, Sabbi, E., et al. 2008, in IAU Symp. 255, ed. L. K. Hunt, S. Madden, & R. Schneider (Cambridge: Cambridge Univ. Press), 381
Tosi, M., Greggio, L., Marconi, G., & Focardi, P. 1991, AJ, 102, 951
Tsujimoto, T., & Bekki, K. 2009, ApJL, 700, L69
Weisz, D. R., Dolphin, A. E., Skillman, E. D., et al. 2013, MNRAS, 431, 364
Westerlund, B. E. 1964, MNRAS, 127, 429
Westerlund, B. E. 1997, The Magellanic Clouds (Cambridge Astrophys. Ser., Vol. 29; Cambridge: Cambridge Univ. Press)
Zaritsky, D., Harris, J., Grebel, E. K., & Thompson, I. B. 2000, ApJL, 534, L53
Zaritsky, D., Harris, J., Thompson, I. B., Grebel, E. K., & Massey, P. 2002, AJ, 123, 855